JOURNAL OF APPLIED POLYMER SCIENCE VOL. 14, PP. 1879–1899 (1970)

Studies on Dry Spinning. II. Numerical Solutions for Some Polymer–Solvent Systems Based on the Assumption that Drying Is Controlled by Boundary-Layer Mass Transfer

YOSHIYUKI OHZAWA and YUTAKA NAGANO, *Katata-Research Institute, Toyobo Co., Ltd., Honkatata, Otsu, Japan*

Synopsis

Numerical solutions of the fundamental equations for dry spinning are obtained by assuming that the rate of the drying of solvent is controlled by the transfer of the solvent vapor at the boundary layer formed outside the filament surface. The polymer–solvent systems for the calculation cover acetate–acetone, poly(vinyl alcohol)–water, polyacrylonitrile–dimethylformamide, and polyurethane–dimethylformamide systems. Quantities necessary for the calculation are summarized. They are material properties (vapor pressures of the solvents, viscosities of the polymer and solvent systems, and so forth) and heat- and mass-transfer coefficients. Mass-transfer coefficients for acetone and dimethylformamide are evaluated by measuring the ratio of heat-transfer coefficient to mass-transfer coefficient based on the method of measuring wet- and dry-bulb temperatures. The variation of the phenomenologic quantities such as solvent content, cross-sectional area, and temperature of the filament along the spinning path is shown in Figure 4.

INTRODUCTION

Obtaining numerical solutions of the fundamental equations for dry spinning derived in a somewhat general form[1] is cumbersome and time consuming without making further simplifying assumptions or discarding physically unimportant equations or terms, even if we rely on a computer. In this paper we focus our attention on the drying process of solvent for simplicity of calculation and try to obtain numerical solutions for the steady state process.

The rate of change of the solvent content within a filament will be controlled according to the stages of drying by either or both of two factors: the transfer of solvent vapor at the boundary layer formed outside the filament surface, and the diffusion of the solvent within the filament. At an early stage of drying, the concentration of the solvent within the filament will be practically uniform and hence the rate of the drying will be exclusively controlled by the former factor. However, as the drying proceeds, the concentration of the solvent at the filament surface will decrease and this will cause the radial distribution of the

solvent concentration within the filament. At this stage, the drying rate of the solvent will gradually come to be controlled by the latter factor.

In this paper, confining our attention to the early stage of the drying, i.e., neglecting the latter factor, we will obtain numerical solutions of the steady state equations for acetate–acetone, poly(vinyl alcohol) (PVA)–water, polyacrylonitrile (PAN)–dimethylformamide (DMF), and polyurethane (PU)–DMF systems for the appropriate spinning conditions.

EQUATIONS

Equation of Solvent Content

At the early stage of the drying we can neglect the diffusion equation, i.e., the microscopic equation[1] of continuity for the solvent in the polymer and solvent mixture, since we do not need to consider the diffusion of the solvent on account of the assumption of radially uniform distribution of the solvent within the filament. Further, in the macroscopic equation[1] of continuity for the solvent we can replace the average solvent content $\langle \omega_S \rangle$ simply by ω_S. Then, the solvent content within the filament is determined by the equation

$$\frac{d\omega_S}{dz} + \frac{2\sqrt{\pi A}}{W_P} M_S N_{S,0} (1 - \omega_S)^2 = 0 \tag{1}$$

where the molar flux $N_{S,0}$ of the solvent is expressed by

$$N_{S,0} = \frac{k_x(x_{S,0} - x_{S,\infty})}{1 - x_{S,0}}. \tag{2}$$

Equations of Cross-Sectional Area and Spinning Tension

Spinning tension F can be represented as a sum of F_W, which represents a constant force acting between the filament and a takeup device, and F_z, which varies along the spinning direction.

The treatment of surface tension given by Ohzawa[1] et al. should be corrected as follows[2]:

Equation of Cross-Sectional Area

$$\ln \frac{A(z)}{A_N} = \ln \frac{1 - \omega_{S,N}}{1 - \langle \omega_S(z) \rangle} - \frac{\rho}{W_P} \int_0^z \frac{(1 - \langle \omega_S(z) \rangle) F(z)}{\langle \beta(z) \rangle} dz$$

Equation of Spinning Tension

$$F = F_W + F_z$$

where

$$F_W = \frac{\ln \frac{A_N}{A_W} (1 - \omega_{S,N}) - \frac{\rho}{W_P} \int_0^{zw} \frac{1 - \langle \omega_S \rangle}{\langle \beta \rangle} F_z dz}{\frac{\rho}{W_P} \int_0^{zw} \frac{1 - \langle \omega_S \rangle}{\langle \beta \rangle} dz}$$

and

$$F_z = -\rho(A_W v_W^2 - A v_z^2) + \rho g \int_z^{z_W} A dz - [F_d(z_W) - F_d(z)] + 2\sqrt{\pi}\,[\sigma\sqrt{A}|_{z_W} - \sigma\sqrt{A}|_z]$$

Analysis in melt spinning shows that F_W is dominant when compared with F_z.[3,4] This means that the spinning tension is approximately constant throughout the soldification length of the filament. In dry spinning, however, the length necessary for the drying is longer than the solidification length in melt spinning and the takeup velocity is usually lower than that in melt spinning. Hence, the spinning tension is supposed to be of smaller value. This leads to a question whether the spinning tension can be assumed to be constant throughout the drying length. However, the thinning process due to the spinning tension will be completed at a considerably early stage of the drying, because at a later stage the high viscosity caused by solvent evaporation will not permit the elongational flow. Therefore, the spinning tension will be safely approximated to be constant over this short length where the elongational flow plays a dominant part in thinning processes of the filament.

Moreover, if the term F_z is neglected, the calculation of F_W can be carried out without knowing the value of the cross-sectional area $A(z)$. This simplifies the calculation. With these considerations we assume that the contributions of acceleration, gravity, drag force, and surface tension to the spinning tension are negligible as compared with the force which acts between the filament and the takeup device.

Then, equations of cross-sectional area and spinning tension, respectively, can be written as follows:

$$\ln \frac{A(z)}{A_N} = \ln \frac{1 - \omega_{S,N}}{1 - \omega_S(z)} - \frac{\rho F}{W_P} \int_0^z \frac{1 - \omega_S(z)}{\beta(z)}\, dz \tag{3}$$

$$F = F_W \text{ (constant)} \tag{4a}$$

$$= \frac{\ln \dfrac{A_N}{A_W}\,(1 - \omega_{S,N})}{\dfrac{\rho}{W_P}\displaystyle\int_0^{z_W} \frac{1 - \omega_S(z)}{\beta(z)}\, dz} \tag{4b}$$

$$= \frac{\ln \dfrac{v_W}{v_N}}{\dfrac{\rho}{W_P}\displaystyle\int_0^{z_W} \frac{1 - \omega_S(z)}{\beta(z)}\, dz} \tag{4c}$$

where v_W/v_N in eq. (4c) represents "spinning draw ratio," an analogue of "meltdraw ratio" and "draw ratio" in cold drawing.

Equation of Temperature

In melt spinning the temperature of the filament is controlled predominantly by the boundary-layer heat transfer at the filament surface.[3,4] This implies rapid heat transfer within the filament and hence flat temperature distribution within it. If this condition applies to dry spinning, the temperature $T(z)$ of the filament is given by replacing the average temperature $\langle T(z) \rangle$ and the surface temperature $T_0(z)$ simply by $T(z)$ in the macroscopic equation of temperature[1]:

$$\rho C_p v_z \frac{dT}{dz} = 2\sqrt{\frac{\pi}{A}} [h(T_\infty - T) - L_S N_{S,0}]. \tag{5}$$

Heat- and Mass-Transfer Coefficients

As stated above, the calculations in this paper are based on the assumption that both solvent content and temperature of the filament are controlled exclusively by the rate of transfers of solvent vapor and heat at concentration and thermal boundary layers formed on the filament surface. Therefore, it is necessary to make as correct an estimation as possible for heat- and mass-transfer correlations. For this purpose we use the equivalent addition method presented by Sano et al.[5] and adopt the correlation for heat transfer to which entrained convective flow caused by the movement of the filament and forced turbulent flow contribute additively (we neglect the contribution of free convection).

Correlation for heat transfer to which entrained convection and forced convection parallel to the filament contribute additively:

$$\mathrm{Nu} = 0.35 + 0.146\ (\mathrm{Re_P} + R)^{0.50} \tag{6}$$

where

$$R = (1.03\ \mathrm{Re_W}^{0.36} - 0.685)^2 \tag{7}$$

and $\mathrm{Re_P}$ and $\mathrm{Re_W}$ are Reynolds numbers based on velocities of parallel forced convection, $U_{P,\infty}$ and the running filament, v_z, respectively.

Correlation for heat transfer to which entrained convection and forced convection perpendicular to the filament contribute additively:

$$\mathrm{Nu} = 0.35 + 0.50\ (\mathrm{Re_C} + R)^{0.50} \tag{8}$$

where

$$R = (0.30\ \mathrm{Re_W}^{0.36} - 0.20)^2 \tag{9}$$

and $\mathrm{Re_C}$ is the Reynolds number based on the velocity of perpendicular forced convection, $U_{C,\infty}$.

If we rewrite these equations in a form convenient for calculation, we get a heat-transfer coefficient for the state where entrained convection is superimposed on forced parallel convection as follows:

$$h = \frac{0.886\lambda^*}{\sqrt{A}} \left[0.35 + 0.146\ (1.129\ \frac{\sqrt{A}\, U_{P,\infty}}{\nu^*} + R)^{0.50} \right] \tag{10}$$

where

$$R = \left[1.076 \left(\frac{\sqrt{A}\, V_z}{\nu^*} \right)^{0.36} - 0.685 \right]^2. \tag{11}$$

For the state where entrained convection is superimposed on forced perpendicular convection, we get a heat-transfer coefficient

$$h = \frac{0.886\lambda^*}{\sqrt{A}} \left[0.35 + 0.50(1.129 \frac{\sqrt{A}\, U_{C,\infty}}{\nu^*} + R)^{0.50} \right] \tag{12}$$

where

$$R = \left[0.313 \left(\frac{\sqrt{A}\, V_z}{\nu^*} \right)^{0.36} - 0.20 \right]^2. \tag{13}$$

It should be noted that eqs. (10)–(13) will give more correct correlations than those described previously.[1]

Mass-transfer coefficients will be obtained by substituting eq. (10) or eq. (12) into the expression derived by assuming analogy between heat and mass transfer[1,6]:

$$k_x = \frac{c^* D_{AS}^*}{\lambda^*} \left(\frac{\mathrm{Sc}}{\mathrm{Pr}} \right)^{1/2} h \tag{14a}$$

$$= \frac{1}{\tilde{C}_p^*} \left(\frac{\mathrm{Pr}}{\mathrm{Sc}} \right)^{1/2} h \tag{14b}$$

To carry out the calculation, we have to know the k_x/h values for air–solvent vapor systems. These values will be given in the next section.

Material Properties

Since experimental data on vapor pressures of solvents are unavailable for the present polymer–solvent systems in the temperature and concentration range encountered in dry spinning, we proceed by assuming the following: (1) equilibrium relationship of the solvent between the solution phase and the gas phase is established at the filament surface immediately after the solution leaves the spinneret; (2) this equilibrium relationship obeys Flory's expression for athermal polymer solution; (3) the total pressure in the gas phase is equal to 1 atm; and (4) the surrounding air and the solvent vapor constitute an ideal gas mixture.

Then the equilibrium relationship can be expressed by

$$x_S = P_S \omega_S e^{(1 - \omega_S)} \tag{15}$$

where the vapor pressure P_S for pure solvent is expressed by the following Antoine equation:

$$\log_{10} P_S = A - \frac{B}{T + C} \tag{16}$$

where P_S and T are expressed in units of [atm] and [°C], respectively, and the constants A, B, and C for each solvent are collected in Table I.

Data on the Trouton viscosity are also unavailable for the polymer–solvent systems studied. However, we can proceed by making use of the data on shear viscosity. This is based on the fact that the velocity gradient at the elongational flow stage of thinning of the filament is of low value, namely of the order of 10 sec^{-1} at most. In this region of small velocity gradient, a polymer solution may behave as an incompressible Newtonian liquid, for which the Trouton viscosity is three times the shear viscosity.[10,11] The law for an incompressible Newtonian liquid has been confirmed in molten polystyrene at low deformation stresses.[12] Therefore, if we make use of this law for obtaining the Trouton viscosity, our aim is to find expressions for low shear viscosity.

Low shear viscosity, η_0, varies with degree of polymerization, P_n, polymer concentration, ω_P, and temperature, T. A break is commonly observed in plots of log η_0 versus log P_n for many amorphous polymer solutions.[13] In the higher viscosity region of this break, namely in the entanglement region, it has been observed that η_0 is proportional to $P_n^{3.4}$ at fixed polymer concentration and that this proportionality is independent of temperature.

TABLE I
Values of Constants A, B, and C for eq. (16)

	A	B	C
Acetone[7]	3.86949	1030.96	209.83
Water[8]	4.9289	1572.53	219
DMF[9]	3.5505	1073.9	152.24

A break has also been observed in plots of log η_0 versus log ω_P for several polymer solutions.[13] A power dependence of η_0 on ω_P at fixed P_n in the entanglement region is generally in the region of 5 to 6 irrespective of temperature.

Temperature dependence of η_0 is usually expressed by flow activation energy ΔE, which does not vary with P_n and ω_P in the entanglement region.[13]

The PVA–water system is one of the typical examples having these commonly observed features of low shear viscosities.[14] In acetate–acetone[15,16] and PAN–DMF[17] systems, however, breaks in plots of log η_0 versus log ω_P were observed to occur rather bluntly and hence the power dependence of η_0 on ω_P increased gradually with polymer concentration. Moreover, flow activation energy was observed to increase with increasing P_n and ω_P.

However, our interest is in the narrow range of concentration and temperature around the initial state of the dope, because the elongational flow occurs at the early stage of spinning, namely, where the state of the dope does not appreciably deviate from the initial condition.

With these considerations we seek the expressions for low shear viscosities in the form

$$\eta_0 = KP_n^m (1 - \omega_S)^n \exp (\Delta E/RT) \quad (17)$$

where K, m, n, and ΔE may be fixed as constants characteristic of the system. The values of these constants for the systems in consideration can be summarized on the basis of the experimental results in the published papers.[14-18] They are tabulated in Table II, in which the range of applicability of the variables P_n, ω_S and T are also written.

TABLE II
Values of Constants K, m, n, and ΔE for Eq. (17) and Range of Applicability of Variables P_n, ω_S, and T

	K, poises	m	n	ΔE, cal/mole	P_n[a]	ω_S	T, °C
Acetate–acetone[15,16]	6.6×10^{-12}	3.7	7	1.36×10^4	160–240	0.70–0.75	25–85
PVA–water[14]	3.24×10^{-10}	3.5	6	7.65×10^3	600–2200	0.83–0.90	20–55
PAN–DMF[17]	3.78×10^{-10}	3.5	7	8.60×10^3	~1800	0.74–0.85	60–120
PU–DMF[18]	2.81×10^{3a}	—	9	6.86×10^3	—	0.70–0.74	30–60

[a] The P_n dependence of the viscosity was not measured for the PU–DMF system. Therefore, the factor of P_n^m is included in the value of K.

Other physical properties of the systems are assumed to be constant: the density ρ and the specific heat C_p at constant pressure of the filament are assumed to have common values for each system, i.e., 1.0 g/cm³ and 0.5 cal g^{-1} °C^{-1}, respectively. Values of heat of vaporization of pure solvents at their boiling points are shown in Figure 6 in the Appendix.

EXPERIMENTAL DETERMINATION OF h/k$_x$ VALUES

The h/k_x values can be calculated from eq. (14), if binary diffusivities D_{AS} for air–solvent vapor systems are known. Of the data on D_{AS} for the solvents discussed in this paper, those for water are available but not for acetone and DMF, as far as we know. For this reason we measured h/k_x values for these solvents by utilizing the method of measuring wet- and dry-bulb temperatures, which was studied by Mizushina and Nakajima.[6]

According to film theory on simultaneous heat and mass transfer,[19] the h/k_x value is related to wet- and dry-bulb temperatures, T_∞ and T_0, respectively, by the equation

$$\ln\left[1 + \frac{x_{S,0} - x_{S,\infty}}{1 - x_{S,0}}\right] = \frac{h}{k_x \tilde{C}_{p,S}} \ln\left[1 + \frac{\tilde{C}_{p,S}(T_\infty - T_0)}{L_{ST}}\right] \quad (18)$$

where $\tilde{C}_{p,S}$ is heat capacity at constant pressure per mole of solvent vapor and L_{ST} is heat of vaporization per mole of pure solvent at temperature T_0. This equation means that we can calculate the h/k_x value, if we measure wet- and dry-bulb temperatures for a given solvent.

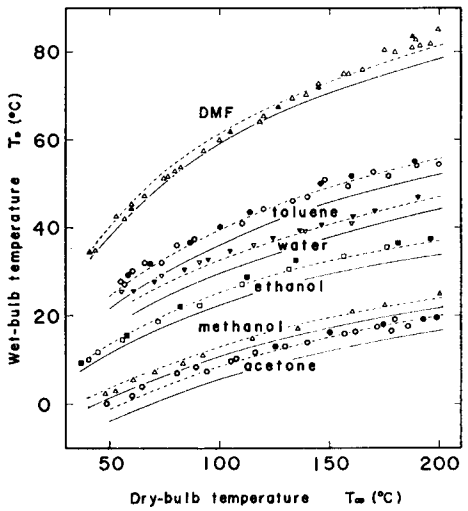

Fig. 1. Dry- and wet-bulb temperatures for acetone, DMF, and standard solvents: (●,○) acetone; (△,▲) methanol; (■,□) ethanol; (▼,▽,) water; (●,○) toluene; (▲,△) DMF. Closed and open symbols represent fresh air flow velocities of 2 m/sec and 5 m/sec, respectively. Calculations: (—) from eq. (18); (– – –) from eq. (19), with $\alpha = 1.23$. The h/k_x values used in the calculation for acetone and DMF are 11.6 and 7.5 cal mole^{-1} °C^{-1}, respectively. See Appendix for h/k_x values of standard solvents.

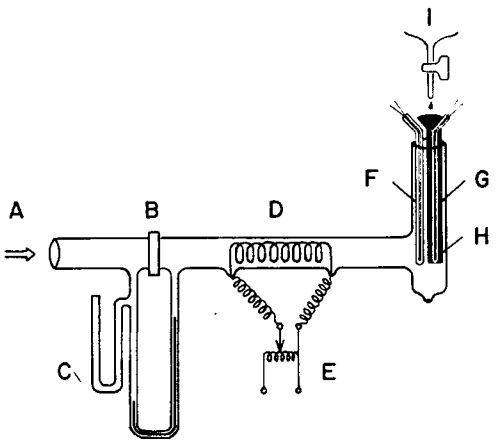

Fig. 2. Apparatus for measurement of wet- and dry-bulb temperatures: (A) fresh air; (B) orifice; (C) manometer; (D) electric heater; (E) transformer; (F) dry-bulb thermometer; (G) wet-bulb thermometer; (H) wick; (I) solvent.

First we calculate wet-bulb temperatures by eq. (18) for some standard solvents for which physical constants necessary for the calculation are known. Methanol, ethanol, water, and toluene are chosen as standard solvents. Calculated wet-bulb temperatures for fresh air flow ($x_{S,\infty} = 0$) are drawn with solid lines against dry-bulb temperatures in Figure 1 (see Table V in the Appendix for physical constants of the solvents).

The experimental apparatus was of the same type as that used by Mizushina and Nakajima.[6] Its schematic description is given in Figure 2. Wet- and dry-bulb temperatures were measured with a pair of thermocouples molded in fine, long glass tubes (3 mm diam.), one of which (dry bulb) was bare and the other (wet bulb) was covered with a wick saturated with pure solvent. Velocities of fresh air ranged from 2 m/sec to 5 m/sec and temperatures ranged from 40°C to 200°C. Wet-bulb temperatures did not vary with air velocities higher than 2 m/sec. Experimentally obtained wet-bulb temperatures for standard solvents are plotted with closed (2 m/sec) and open (5 m/sec) symbols against dry-bulb temperatures in Figure 1.

Before we compare these experimental results with predictions of eq. (18) for standard solvents, we should remind of some of the assumptions made for its derivation: (1) eq. (18) is derived for the boundary condition of one-dimensional steady flow along a flat surface; (2) air velocity is high enough that the thermometer readings are unaffected by radiation and by heat conduction along the thermometer; (3) heat and mass transfers take place through the same area of the wick surface.

The rigorous examination of the applicability of eq. (18) to the boundary condition in our experiment is beyond our scope. However, we proceed by assuming its applicability, for, as is seen in Figure 1, the relationship between wet- and dry-bulb temperatures for the standard solvents shows the same shape of curve for the experiment and the theoretical prediction. Furthermore, if we introduce a correction factor α into eq. (18), the corrected equation represents satisfactorily the experimental relationship between wet- and dry-bulb temperatures, as will be discussed below.

The wet-bulb thermometer was surrounded by the portions of the apparatus heated nearly to dry-bulb temperature T_∞. Therefore, heat transports due to radiation and conduction from the surroundings might not be negligible. Furthermore, as Mizushina and Nakajima[6] pointed out, some local portions of the wick surface must be in the dry state for the liquid solvent to come up to the wick surface by capillary action. This means that the effective area of the wick surface which contributes to mass transfer is somewhat less than the area for heat transfer.

These deviations in the actual experiment from assumptions (2) and (3) would be the sources of a higher wet-bulb temperature than that predicted by eq. (18). In order to eliminate this discrepancy between experiment and theory and in order to obtain an expression which will represent experimental results satisfactorily, we introduce a correction factor α into eq. (18) in the analogous fashion as did Mizushina and Nakajima:

$$\ln\left[1 + \frac{x_{S,0} - x_{S,\infty}}{1 - x_{S,0}}\right] = \frac{h}{k_x \bar{C}_{p,S}} \ln\left[1 + \frac{\alpha \bar{C}_{p,S}(T_\infty - T_0)}{L_{ST}}\right] \quad (19)$$

where α is larger than unity and is considered to be a characteristic quantity of the apparatus utilized. If we put $\alpha = 1.23$ in eq. (19) and calculate wet-bulb temperatures for the standard solvents, the calculated curves (shown with broken lines in Fig. 1) fit most satisfactorily the experimental results.

Hence, it follows that the characteristic value of α for this apparatus is 1.23 and that eq. (19) represents satisfactorily enough the experimental results.

If we assume that the experimental relationship between wet- and dry-bulb temperatures for acetone and DMF (also shown in Fig. 1) measured with the same apparatus are also represented by eq. (19) with $\alpha = 1.23$, we can calculate the h/k_x values for these solvents by substituting experimental T_0 and T_∞ values into eq. (19). These calculated values of h/k_x are listed in Table III at several dry-bulb temperatures. It is seen that the h/k_x

TABLE III
Experimentally Obtained h/k_x Values for Acetone and DMF

	Acetone		DMF	
Dry-bulb temp °C	Wet-bulb temp °C	h/k_x, cal mole^{-1} °C^{-1}	Wet-bulb temp °C	h/k_x, cal mol^{-1}°C^{-1}
200	19.4	11.4	83.4	8.1
180	17.5	11.3	79.8	7.9
160	15.6	11.4	75.7	7.5
140	13.7	11.5	72.1	7.7
120	11.4	11.7	66.0	6.8
100	8.8	11.8	60.6	6.8
80	5.8	12.1	53.0	6.3[a]
Average	—	11.6	—	7.5

[a] Omitted from averaging.

value for acetone varies very slightly with temperature, while that for DMF depends somewhat on temperature. However, we neglect temperature dependence of h/k_x values and adopt values averaged over the experimental range of temperature. These values are 11.6 cal mole^{-1} °C^{-1} for acetone and 7.5 cal mole^{-1} °C^{-1} for DMF. These averaged values are used in the present calculation for dry spinning. Calculated curves of wet-bulb temperatures by substituting these values into eq. (18) are also shown in Figure 1 with solid lines together with the curves by eq. (19) with $\alpha = 1.23$ (broken lines).

It may be worth noting that if, instead of eq. (14) for the calculation of wet-bulb temperature, we use the expression

$$h/k_x = \bar{C}_p^* \left(\frac{\mathrm{Sc}}{\mathrm{Pr}}\right)^{2/3}, \tag{20}$$

which is frequently referred to in textbooks of heat and mass transfer, the experimentally obtained wet-bulb temperatures for ethanol and toluene lie lower than those predicted by eqs. (18) and (20). This fact contradicts our expectation stated before, since α becomes less than unity in this case. Therefore, as Mizushina and Nakajima suggested, eq. (14) is more suitable for the expression of h/k_x value than eq. (20) in the range of Pr and Sc numbers between 0.5 and 2.5.

RESULTS AND DISCUSSION

The spinning conditions for the polymer–solvent systems must be given for the calculation to be carried out. These can be determined by reference to the results reported in the papers.[20–26] Table IV shows the spinning conditions for which calculations were carried out. As is seen, the conditions except degree of polymerization of polymer, dope temperature, and air flow temperature are made common to all the systems in order to make it easy to compare the calculated results among the systems. Values of degree of polymerization and dope temperature are determined so that dope shear viscosities range between 100 and 300 poises. Air flow temperature is determined mainly from the point of drying of the solvent.

TABLE IV
Spinning Conditions for Example Calculations

	Acetate–acetone[20]	PVA–water[21,22]	PAN–DMF[23–25]	PU–DMF[26]
Degree of polymerization P_n	200	1200	1350	—
Dope output W, g/sec	2×10^{-2}	2×10^{-2}	2×10^{-2}	2×10^{-2}
Mass fraction of solvent in the dope $\omega_{S,N}$	0.74	0.74	0.74	0.74
Initial cross-sectional area A_N, cm²	1×10^{-3}	1×10^{-3}	1×10^{-3}	1×10^{-3}
Final cross-sectional area A_W, cm²	2×10^{-5}	2×10^{-5}	2×10^{-5}	2×10^{-5}
Dope temperature T_N, °C	55	90	100	120
Air temperature T_∞, °C	70	200	200	250
Mole fraction of solvent vapor in air flow $x_{S,\infty}$	0	0	0	0
Velocity of parallel air flow $U_{P,\infty}$, cm/sec	50	50	50	50

Iterative method makes it possible to obtain numerical solutions for a set of equations of solvent content (eq. (1)), spinning tension (eq. (4)), cross-sectional area (eq. (3)), and temperature (eq. (5)) of the filament.

The steps can be summarized as follows:

(1) Assume appropriate values for A and T as starting approximations (the assumed values are denoted by $A^{(0)}$ and $T^{(0)}$). In the present computation $A^{(0)}$ and $T^{(0)}$ were chosen to be A_N and T_0 (wet-bulb temperature corresponding to T_∞ and $x_{S,\infty}$).

(2) Calculate ω_S from eq. (1) with $A^{(0)}$ and $T^{(0)}$ as data for this equation. The obtained ω_S is denoted by $\omega_S^{(1)}$.

(3) Calculate spinning tension by substituting $\omega_S^{(1)}$ and $T^{(0)}$ into eq. (4) and then calculate cross-sectional area from eq. (3). The obtained results are denoted by $F_W^{(1)}$ and $A^{(1)}$, respectively.

(4) Calculate temperature of the filament by substituting $\omega_S^{(1)}$ and $A^{(1)}$ into eq. (5). The result is denoted by $T^{(1)}$.

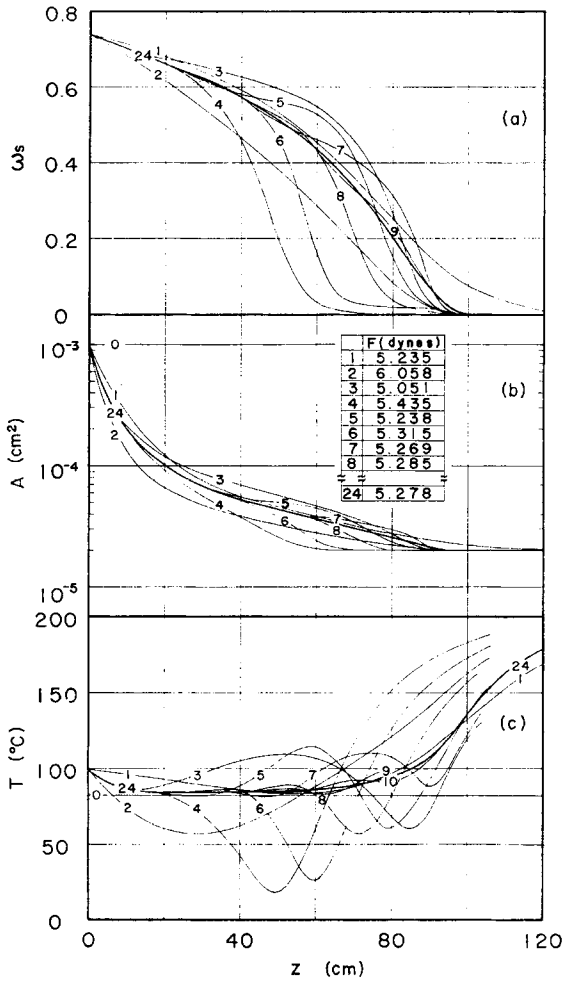

Fig. 3. Results of first several and last iterations for PAN–DMF system: (a) mass fraction of the solvent ω_S; (b) cross-sectional area A and spinning tension F; (c) temperature T. Numerals (1,2,... 24) in the figure indicate the number of approximations.

(5) Update the values of $\omega_S^{(1)}$, $F_W^{(1)}$, $A^{(1)}$, and $T^{(1)}$ by repeating steps (2), (3), and (4) by substituting the newest values of ω_S, F_W, A, and T into the corresponding equations.

(6) Stop the calculation if the convergence criteria are satisfied.

In order to make the convergence faster, it is desirable to use more previous results as well as the corrected ones with appropriate weight as the new data for the equations. Usually 20 to 30 repetitions were required in obtaining the results within 0.1% accuracy of coincidence.

Figure 3 shows how the convergence proceeds with increasing number of repetitions for the PAN–DMF system (figures in Fig. 3 indicate the number of repetitions). In this case the new ω_S and T were averages of the previous

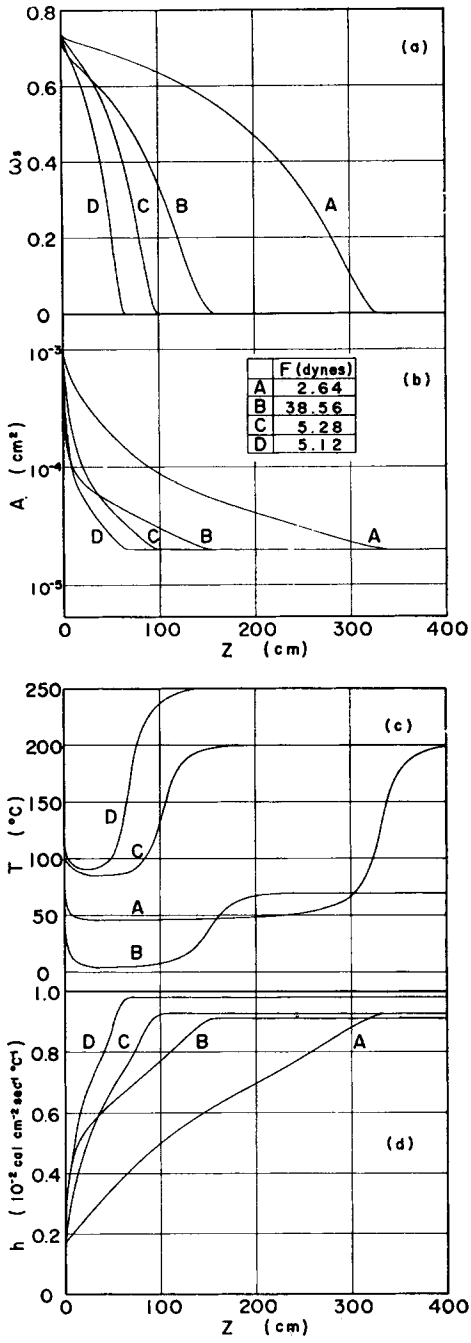

Fig. 4. Final results for systems studied: (a) mass fraction of solvent ω_S, (b) cross-sectional area A and spinning tension F; (c) temperature T; (d) heat-transfer coefficient h; (A) PVA–water system; (B) acetate–acetone system; (C) PAN–DMF system; (D) PU–DMF system.

value and the corrected one. After 24 repetitions the results were obtained within 0.1% accuracy of coincidence for this system.

Figure 4 shows the final results of repetitions for the systems studied. Figure 4a shows the change of mass fraction of the residual solvent in the filament along the spinning direction. The length required for the drying of solvent differs largely among the systems in spite of the same rate of dope output from the spinneret. These differences arise from the variety of physical properties (vapor pressure of solvent, heat of vaporization, and so forth) and spinning conditions (mainly air flow temperature). The greatest length necessary for the drying of the solvent seen in the PVA–water system is ascribable to the large value of heat of vaporization per mass of water, i.e., about 5 times larger than those of other solvents. Actually, the calculation for the "hypothetical solvent" whose heat of vaporization is 100 cal/g (similar value to other solvents) and whose other physical properties are the same as those of water indicates that the length for the drying in the system composed of PVA and this "hypothetical solvent" decreases by a factor of about 4 for the same spinning conditions as for the PVA–water system (not shown in Fig. 4).

The curve for the acetate–acetone system shows rapid decrease of the solvent in the very short range below the spinneret. This is because the dope temperature is very near to the boiling temperature of acetone.

The drying of the solvent in the PU–DMF system is completed in a shorter length than that in the PAN–DMF system. This is due to the fact that air temperature for the former system (250°C) is higher than that for the latter (200°C), since the same solvent is used for both systems.

Figure 4b shows spinning tension and change of cross-sectional area of the filament in the spinning direction. The thinning process near the spinneret arises primarily from the elongational flow caused by the spinning tension, while that at a later stage arises primarily from the evaporation of solvent. In the PVA–water system, for instance, the mass fraction of the solvent decreases only to 0.64 at the distance of 1 m from the spinneret from the initial value of 0.74, whereas the decrease of the cross-sectional area of the filament is seen to be very large at the same distance, i.e., from the initial value of 1.0×10^{-3} cm^2 to 8.8×10^{-5} cm^2. It is concluded, therefore, that the contribution of the second term in eq. (3), i.e., the term of the elongational flow, is predominant to the thinning process of the filament in this region.

On the other hand, the cross-sectional area of 4.0×10^{-5} cm^2 at the distance of 2 m from the spinneret decreases to half its value of 2.0×10^{-5} cm^2 at the takeup position, while the weight fraction of the residual solvent decreases from 0.47 to 0. Therefore, it follows that the thinning in this region is due predominantly to the evaporation of the solvent.

The cross-sectional shape of the dry-spun filament is considered to be largely influenced by the perimeter of the cross section of the filament at the stage where the filament attains such a viscosity level as allows no further elongational flow of the filament. The thinning of the filament thereafter

will be caused not by the uniform contraction of the surface while holding the circular shape of the cross section but by the irregular and spontaneous collapse of the surface whose peripheral length is held unchanged. Therefore, if the residual solvent content is large at the stage where the perimeter is determined, the extent of the collapse of the surface caused by the evaporation of the solvent will be great and therefore the irregularity of the cross-sectional shape of the dry-spun filament will be large.

On this ground it will be possible to roughly presume the cross-sectional shape of the dry-spun filament by considering Figures 4a, 4b, and 5 at the same time. In the acetate–acetone system, for instance, it is seen that the viscosity increases very rapidly as compared with other systems. Therefore, a considerable amount of the solvent will remain within the filament at the stage where its peripheral length is practically determined. This will cause a more irregular shape of the cross section of the dry-spun filament in this system than in other polymer–solvent systems.

Spinning tension arises from the viscous resistance of the elongational flow. It increases both with the Trouton viscosity and the parallel velocity gradient. In the acetate–acetone system it has the high value of 38.56 dynes due to the large viscosity value and the high velocity gradient (see also Fig. 5). In the PVA–water system, on the other hand, spinning tension has the small value of 2.64 dynes because of small values of both factors. In melt spinning it is known that when the spinning tension is great, so is the degree of orientation of polymer chains.

Figure 4c shows the temperature of the filament. Its decrease immediately after the emerging of the dope from the spinneret comes from the heat loss caused by the evaporation of the solvent. However, it does not reach, though gets close to, the corresponding wet-bulb temperature. This is because the activity of the solvent falls from unity according to Flory's expression for athermal solution, (15).

When the mass fraction of the residual solvent attains the value of about 0.3 after a nearly constant region of the temperature has passed, the filament temperature gradually increases toward the air flow temperature. Then its rapid increase occurs when the mass fraction becomes about 0.2.

Figure 4d shows the calculated results for the heat-transfer coefficients. According as the filament leaves the spinneret, the entrained air flow caused by the running of the filament is superimposed on the forced convective air flow. This effect makes the heat-transfer coefficient gradually larger. Its final value at the position where the evaporation of the solvent is completed attains about 5 times its initial value. Slight differences in the heat-transfer coefficients at the final stage among the systems come from slightly different physical constants at the boundary layer due to different air temperatures.

As has been seen, the value of the heat-transfer coefficient is not given as one of the spinning conditions but is determined by solving the set of macroscopic balance equations, since it depends on the state of the filament, for example, the running velocity of the filament.

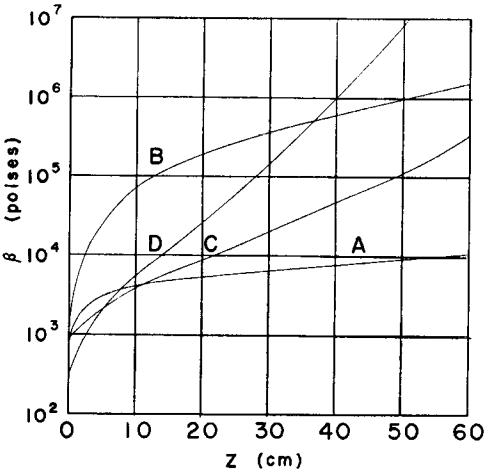

Fig. 5. Calculated results of Trouton viscosity β at early stage of drying: (A) PVA–water system; (B) acetate–acetone system; (C) PAN–DMF system; (D) PU–DMF system.

Figure 5 shows the calculated values of the Trouton viscosities near the spinneret position. It is seen that they increase rapidly after the dope has left the spinneret. This increase is due to the decrease of the solvent concentration and to the decrease of the filament temperature. This increase of viscosity promises the spinnability of the filament in the sense that it prevents the scission of the filament which would be caused by the elongational flow in the course of the thinning process.

CONCLUSIONS

Since dry spinning is a process involving a two-component system, a new aspect arises concerning the drying of solvent when compared with melt spinning, which involves a one-component system. If it is assumed that the rate of drying of the solvent is controlled exclusively by the transfer of the solvent vapor at the boundary layer formed on the filament surface, it suffices to take account of only macroscopic balance equations among the balance equations given in the first paper of this series on dry spinning.[1] Example calculations were carried out by giving the so-called spinning conditions as the initial conditions for the macroscopic equations for some polymer–solvent systems which are actually subjected to dry spinning. Common features to the systems are seen in the variation of the phenomenologic quantities such as solvent content, cross-sectional area, spinning tension, and temperature of the filament along the spinning path. Differences among the systems are also seen, however. They are caused by differences in the properties of polymer–solvent systems, especially solvent properties such as vapor pressure, heat of vaporization, and mutual diffusion coefficient in its vapor–air system.

The analysis given above is based on the assumption that thermodynamic changes like phase separation do not take place during the process or they do not substantially affect phenomenologic aspects even if they occur. However, the phenomenologic analysis like this will be very important in the sense that it offers a great deal of technical or operational information concerning the selection of solvent, the design of the spinning column, the determination of spinning conditions, and so forth.

Molecular aspects like the orientation of polymer chains are not considered in this analysis. Properties of dry-spun filament, however, are largely influenced by such molecular factors as the orientation or the coagulation state of polymer chains. These factors, on the other hand, are controlled by phenomenologic quantities in the course of the formation of fibrous structure.

In this sense it is important to calculate the phenomenologic quantities as exactly as possible in order to be able to infer the properties of dry-spun filaments. Furthermore it was shown that one can infer from the calculation such macroscopic properties of dry-spun filament as its cross-sectional shape.

For a deeper understanding of the dry spinning process it will be useful to know how phenomenologic quantities are affected by spinning conditions. The solution for this problem will be given in a subsequent paper.

As drying of the solvent proceeds, the gradient of the solvent concentration in the radial direction in the filament will occur on account of the finiteness of the value of the mutual diffusion coefficient in the polymer–solvent system. This means that the rate-controlling factor of the drying is gradually switched to the diffusional movement of the solvent within the filament. Therefore, at a later stage of the drying, the solvent content in the filament is expected to be larger than that calculated in this paper. In order to know this effect, one must solve the diffusion equation, namely the microscopic equation of mass balance for solvent. For this, the diffusion coefficients for polymer–solvent systems must be measured. The measurement on diffusion coefficients and the numerical calculations based on this measurement will be described later.

Nomenclature

A	cross-sectional area, cm^2
C_p	specific heat at constant pressure, cal g^{-1} $°C^{-1}$
D_{AS}	binary diffusivity for air and solvent vapor system, cm^2/sec
F	spinning tension, dynes
F_d	total drag force, dynes
L_S	heat of vaporization of pure solvent at its boiling temperature, cal/mole
M_S	molecular weight of solvent, g/mole
$N_{S,0}$	molar flux of solvent at the filament surface with respect to stationary coordinates, moles cm^{-2} sec^{-1}
Nu	Nusselt number, dimensionless

P_n degree of polymerization, dimensionless
Pr Prandtl number, dimensionless
P_S vapor pressure of pure solvent, atm
Re Reynolds number, dimensionless
Sc Schmidt number, dimensionless
T –temperature, °C
$U_{C,\infty}$ velocity of perpendicular air flow, cm/sec
$U_{P,\infty}$ velocity of parallel air flow, cm/sec
W_P mass flow rate of polymer g/sec
c total molar density, moles/cm^3
g gravitational acceleration, cm/sec^2
h heat-transfer coefficient, cal cm^{-2} sec^{-1} °C^{-1}
k_x mass-transfer coefficient, moles cm^{-2} sec^{-1}
v_z z-component of mass-average velocity, cm/sec
x_S mole fraction of solvent, dimensionless
z cylindrical axial coordinate, cm
β Trouton viscosity, poises
η_0 low shear viscosity, poises
λ thermal conductivity, cal cm^{-1} sec^{-1} °C^{-1}
ν kinematic viscosity, cm^2/sec
ρ density, g/cm^3
σ surface tension, dynes/cm
ω_S mass fraction of solvent, dimensionless

Overline:
$\sim$ per mole

Superscripts:
* mean value with respect to boundary layer

Subscripts:
N at $z = 0$
S solvent
W at the windup roll (at $z = z_W$)
0 at the filament surface
∞ air flow

APPENDIX

Physical Constants Used for Calculation of Wet- and Dry-Bulb Temperatures

The values of h/k_x, L_{ST}, $\tilde{C}_{p,S}$, and vapor pressure of the solvents must be known for the calculation of wet- and dry-bulb temperatures by eq. (18).

The h/k_x value can be calculated by eq. (14a) or eq. (14b), if physical constants such as binary diffusivity D_{AS}* for air–solvent vapor system, molar density c*, thermal conductivity λ*, heat capacity $\tilde{C}_p$*, and kinematic viscosity ν* at the boundary layer are known. The temperature dependence of the binary diffusivity D_{AS} may be evaluated by the equation

$$D_{AS} = D_{AS}^{(0)} \left(\frac{T}{T_{(0)}} \right)^m \tag{A1}$$

TABLE V
Physical Constants for Calculation

Solvents	$\bar{C}_{p,S}$, cal mole^{-1} °C^{-1}	Parameters for eq. (A1)		Parameters for eq. (A2)			h/k_x, cal °C^{-1} mole^{-1}	
		$D_{AS}^{(0)}$ cm^2/sec	m	T_b, °C	T_c °C	L_S, cal/mole	calculated from eq. (14)	calculated from eq. (26)
Methanol	15	0.1325	2.0	(64.7)	(240.0)	(8420)	8.1	8.5
Ethanol	21	0.1016	2.0	(78.5)	(243.0)	(9410)	9.6	10.7
Water	8.6	0.220	1.75	(100.0)	(374.2)	(9717)	6.5	6.3
Toluene	45	0.0709	2.0	110.6	320.8	8000	11.1	12.9
Acetone	20	—	—	56.5	235	6940	—	—
DMF	26	—	—	153	373[a]	8480	—	—

[a] Estimated by Lydersen's method.

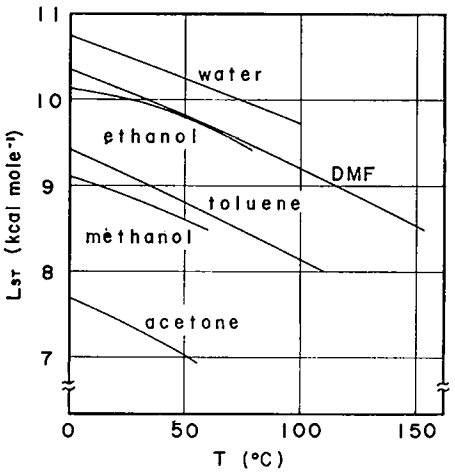

Fig. 6. Heat of vaporization of solvents used in calculation of wet- and dry-bulb temperatures from eqs. (18) and (19). Values for toluene, acetone, and DMF were evaluated from eq. (A2).

where $D_{AS}^{(0)}$ is the diffusivity at $T_{(0)} = 273$ (°K) and 1 atm total pressure and m is a constant characteristic of the system. Values of $D_{AS}^{(0)}$ and m are listed in Table V for the standard solvents. Other constants necessary for the calculation of eq. (14) may be substituted by those for air by assuming that the amount of the solvent vapor at the boundary layer is small enough so that it can be neglected in evaluating the physical properties. The temperature dependence of the h/k_x values calculated by using these constants is very slight in the temperature range of 20° to 150 °C. Thus the h/k_x values for the standard solvents can be represented by the average values over this range. These are listed in Table V, in which those calculated by eq. (20) are also listed.

Figure 6 shows the temperature dependence of heat of vaporization per mole of pure solvent. For toluene, acetone, and DMF, the data on heat of vaporization are available only at their boiling points. Therefore, the curves for these solvents are the results of evaluation in terms of the equation

$$L_{ST} = L_S \left(\frac{T_c - T}{T_c - T_b} \right)^{0.38} \tag{A2}$$

where T_b and T_c are boiling and critical temperatures, respectively, and L_S is the heat of vaporization of the solvent at T_b. These three values are also listed in Table V.

References

1. Y. Ohzawa, Y. Nagano, and Y. Matsuo, *J. Appl. Polym. Sci.*, **13**, 257 (1969).
2. Y. Ohzawa, Y. Nagano, and T. Matsuo, Proc. 5th International Congress on Rheology, 1968, Kyoto.
3. S. Kase and T. Matsuo, *J. Polym. Sci. Part A*, **3**, 2541 (1965).
4. S. Kase and T. Matsuo, *J. Appl. Polym. Sci.*, **11**, 251 (1967).
5. Y. Sano and N. Yamada, *Kagaku Kogaku*, **30**, 997 (1966).
6. T. Mizushina and M. Nakajima, *Kagaku Kikai*, **15**, 30 (1951).
7. V. V. Sokolov, L. P. Zhilina, and K. P. Mishchenko, *Zh. Prikl. Khim.*, **36**, 750 (1963).
8. M. L. Klyueva et al., *Zh. Prikl. Khim.*, **33**, 473 (1960).
9. S. K. Ogorodnikov et al., *Zh. Prikl. Khim.*, **34**, 2441 (1961).

10. F. T. Trouton, Proc. Roy. Soc., *Ser A*, **77**, 426 (1906).
11. A. S. Lodge, *Elastic Liquids*, Academic Press, New York, 1964, p. 98.
12. R. L. Ballman, *Rheol. Acta*, **4**, 137 (1965).
13. R. S. Porter and J. F. Johnson, *Chem. Rev.*, **66**, 1 (1966).
14. S. Onogi, T. Kobayashi, Y. Kojima, and Y. Tanigushi, *Zairyo Shiken*, **9**, 245 (1960).
15. T. Kamiya and K. Hirokawa, *Sen-i Gakkaishi*, **18**, 453 (1962).
16. H. Konishi, *Sen-i Gakkaishi*, **18**, 38 (1962).
17. S. Yugushi, *Kobunshi Kagaku*, **19**, 113 (1962).
18. T. Matsui et al., private communication.
19. R. B. Bird, W. E. Stewart, and E. N. Lightfoot, *Transport Phenomena*, Wiley, New York, 1960, p. 667.
20. T. Kamiya, K. Hirokawa, and T. Imada, *Sen-i Gakkaishi*, **19**, 522 (1963).
21. Y. Sano and S. Nishikawa, *Kagaku Kogaku*, **30**, 245 (1966).
22. M. Uzumaki and H. Suyama, *Sen-i Gakkaishi*, **18**, 321 (1962).
23. M. Takahashi and M. Watanabe, *Sen-i Gakkaishi*, **16**, 458 (1960).
24. Y. Sano and S. Nishikawa, *Kagaku Kogaku*, **30**, 335 (1966).
25. K. Koyano, H. Nagano, and S. Inoue, *Sen-i Gakkaishi*, **22**, 191 (1966).
26. I. Suzuki, *Kobunshi*, **13**, 297 (1964).

Received February 27, 1970
Revised March 2, 1970